ISSN 1063-7729, Astronomy Reports, 2009, Vol. 53, No. 4, pp. 355–368. © Pleiades Publishing, Ltd., 2009.
Original Russian Text © I.M. Chertok, V.V. Grechnev, A.M. Uralov, 2009, published in Astronomicheskiĭ Zhurnal, 2009, Vol. 86, No. 4, pp. 392–405.

Large-Scale Phenomena on the Sun Associated with the Eruption of Filaments Outside Active Regions: the Event of September 12, 1999

I. M. Chertok[1], V. V. Grechnev[2], and A. M. Uralov[2]

[1] *N.V. Pushkov Institute of Terrestrial Magnetism, Ionosphere, and Radio-Wave Propagation, Troitsk, Russia*

[2] *Institute of Solar–Terrestrial Physics of the Siberian Branch of the Russian Academy of Sciences, Irkutsk, Russia*

Received 2008; in final form, July 2, 2008

Abstract—The event of September 12, 1999 is used to analyze large-scale disturbances associated with coronal mass ejections during the eruption of filaments outside active regions. The analysis is based on Hα filtergrams, EUV and soft X-ray images, and coronograph data. The filament eruption occurred in relatively weak magnetic fields, but was accompanied by larger-scale phenomena than flare events. During several hours after the eruption, a large-scale arcade developed, whose bases formed diverging flare-like ribbons. The volume of the event was bounded by an "EIT wave", which was quasi-stationary at the solar surface and expanded above the limb. The event did not have an impulsive component; therefore the "EIT wave" above the limb was a magnetic structure, identified as the front of a coronal mass ejection by virtue of its shape, structural features, and kinematics. Three types of dimmings were observed within the areal of the event, cause by (a) the evacuation of plasma, (b) heating of plasma with its subsequent evacuation, and (c) the absorption of radiation in a system of filaments activated by the eruption. The fact that a dimming appeared due to plasma heating was revealed by its presence in soft X-rays, whereas the four EIT channels did not demonstrate this. This brings into question the correctness of certain conclusions drawn earlier based purely on EIT data. A transformation of magnetic fields brought about by the eruption also occurred in a stationary coronal hole adjacent to the areal of the event. The expansion of the coronal mass ejection was self-similar and characterized by a rapidly decreasing acceleration, which is not taken into account in the widely used polynomial approximation.

PACS numbers: 96.60.qf, 96.60.ph
DOI: 10.1134/S1063772909040088

1. INTRODUCTION

The eruptions of large-scale coronal mass ejections (CMEs) on the Sun are accompanied by a number of extensive phenomena—dimmings, Morton waves and similar coronal disturbances, post-eruptive arcades rooted in bright, extended ribbons, etc. (see, for example, [1, 2]). The scales of these phenomena are comparable to the solar radius.

Dimmings are regions where the brightness of coronal structures in the soft X-ray and extreme UV is reduced over times from several hours to a day. They form near the center of an eruption during the ejection, and can also be observed at and near a large part of the solar surface [3–9]. These were first called "transient coronal holes," but subsequent studies showed that they may have a different nature. It has been suggested that stationary dimmings adjacent to the center of an eruption may be identified with the bases of magnetic structures (ropes) associated with CMEs. The reduced brightness in dimmings can be explained by a decrease in the longitudinal emission measure n^2L due to a reduction of the plasma density in the associated coronal structures. Possible mechanisms include outflows of plasma from magnetic structures opening into interplanetary space as a result of CMEs [10, 11], a reduction of the heating in the upper parts of coronal loops with an inflow of plasma into their bases below [12], and the expansion of structures that are not erupting, leading to a decrease in n^2L if the number of particles they contain remains constant [13]. The absorption of radiation in the low-temperature plasma arriving from a perturbed filament is also possible [13]. The ultimate cause of all these processes is variations in the conditions in the corona as the result of an ejection.

Morton waves are observed in Hα [14] and HeI λ10830 [15] spectroheliograms as arc-like disturbances propagating from the center of an eruption

with speeds of 550–2500 km/s. Outwardly similar coronal disturbances in the extreme UV, and sometimes the soft X-ray, are observed as weakly emitting fronts that either propagate to large distances with low speeds of 250–800 km/s or are quasi-stationary [3, 16–24]. These disturbances are observed both on the solar disk and beyond the disk, in the form of expanding structures. Since they were first discovered using the SOHO/EIT telescope, they received the general name "EIT waves", although not all of them appear to be waves as such. The variety of observational data on these phenomena make it unlikely that they can be explained within a single interpretation.

An explanation of near-surface "EIT waves" as the outer boundaries of expanding bases of CMEs was proposed and developed in [16, 25, 26]. In this model, an "EIT wave" is a region of magnetic reconnection of CME-associated magnetic fluxes and subsequently opening magnetic structures near the solar surface; i.e., it is essentially the outer boundary of an expanding dimming. The similar model [27] invokes volume reconnection of the magnetic fluxes of a CME and the "magnetic carpet" of the quiet Sun. Based on the kinematic similarities between "EIT waves" and Morton waves observed in some events, some researchers have associated both of these phenomenon with a single decelerating disturbance, such as a coronal explosive shock [13, 21, 28]. In some individual cases, "EIT waves" expanding above the limb have been identified with CME front structures [12, 29, 30]. Various combinations of these interpretations have also been considered [31, 32]. It seems likely that the direct cause of the enhanced brightness of wave-like disturbances observed in EUV lines with a relatively narrow range of temperature is an enhancement in the longitudinal emission measure in a region of compression. The brightness in the soft X-ray emission depends directly on both the density and the temperature of the plasma.

Large-scale arcades with extended emitting ribbons at their bases form in the post-eruptive phase. In this stage, the magnetic field in the extended region of the corona blown out by the CME eruption relaxes to an equilibrium state, possibly via magnetic reconnection in extended, high-lying current sheets.

Two classes of eruptive events associated with CMEs are recognized: (1) flares (and filament eruptions) in active regions (ARs) and (2) filament eruptions (protuberances) outside ARs [33]. The indicated large-scale phenomena have been analyzed primarily for eruptions in ARs associated with flares, and precisely such events have been the subject of the majority of the cited studies. At the same time, large-scale disturbances during eruptions outside ARs are relatively poorly studied. For example, little is known about the presence and character of "EIT waves" in such events. Individual properties of large-scale disturbances in such eruptions have been considered in only a few works [12, 30, 34–39]. The analysis of large-scale disturbances during eruptions outside ARs is not only important for studies of the physical characteristics of this class of phenomenon; both classes of eruptions apparently display the same general tendencies, and a number of similar properties may be expected together with their differences. Consideration of the filament eruption outside ARs as a slowed flare-like process without an impulsive phase [33] may also provide detailed information about some processes occurring in eruptive flares. Moreover, CMEs that are not associated with flares are sources of appreciable geomagnetic disturbances with Dst indices reaching −200 nT [40]. Therefore, studies of filament eruptions outside ARs and associated large-scale phenomena are also important for space weather forecasting.

We analyzed large-scale disturbances for approximately 100 eruptions outside ARs during 1996–2006. We present the results of this analysis and the typical characteristics of these large-scale phenomena using the event of September 12, 1999, which was well observed in a number of wavelength ranges, as an example. Section 2 describes the input data and main analysis method used. Sections 3–6 consider the conditions of the filament eruption and properties of the dimmings, the post-eruptive arcade, flare-like ribbons, the CME, and the detected coronal disturbance ("EIT wave"), which can be identified in this case with a front structure of the CME. Section 7 generalizes and discusses the results obtained.

2. DATA AND ANALYSIS METHOD

Studying the event of September 12, 1999, we carried out a joint analysis of various data. Hα filtergrams obtained at the Big Bear Observatory with a time interval of as little as 30 s, kindly provided by V. Yurchishin, enabled us to follow the filament eruption in detail. To analyze the filtergrams, it is necessary to align the images, subtract the effect of limb darkening, and enhance the contrast of the images, for which we used procedures available in the SolarSoft program package. The large number of filtergrams (more than 500) and their large format (2032×2028 pixels) required that we take measures to reduce the overall processing time.

In the first stage, the images were reduced to a 256×256 format. Using the IDL procedure "align_cube" (developed by R. Molowny-Horas), we determined the shift of each image relative to a selected reference image. We then used the procedure "background" (A. McAllister) to find the center of

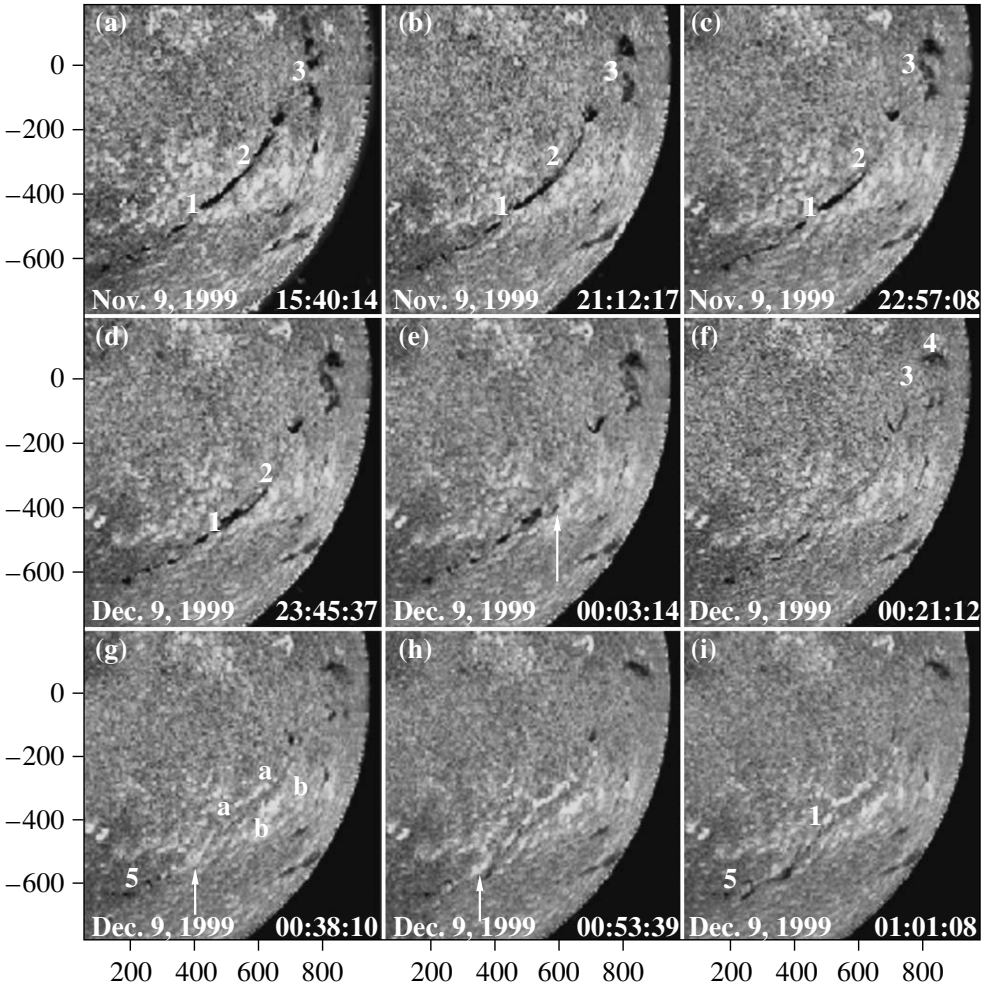

Fig. 1. Hα filtergrams from the Big Bear Observatory illustrating the evolution and eruption of filament 1-2-3, as well as the dynamics of the ribbons aa and bb in the post-eruptive phase. On this and other analogous figures, the axes show distance from the center of the disk in arcseconds. All these and the subsequent images were processed in a non-linear fashion designed to reveal the discussed features.

the reference image reduced by a factor of two, after which each image was centered using "align_cube" and the shifts found in the first step multiplied by the appropriate coefficient. When composing the films, the limb darkening was usually determined by applying "background" to every 10th image (to economize on processing time), and individually for each of the images shown in Fig. 1. Finally, we enhanced the contrast of the images using the procedure "sigrange" (W. Thompson).

Very important information for our study is contained in EUV data obtained with the SOHO/EIT telescope. EIT observations are carried out in the 195 Å channel (dominated by the Fe XII line, characterized by a temperature of 1.3 MK) with cadence of 12 min. In addition, EIT provides images every six hours in two coronal channels at 171 Å (Fe IX/X, 0.9 MK) and 284 Å (Fe XV, 2.0 MK), as well as in the 304 Å channel, which is dominated by radiation from the transition layer (He II, 0.02–0.08 MK and the less intense Si XI coronal component, 1.6 MK) [29, 41].

Dimmings, the post-eruptive arcade, and the ribbons at its base were studied using images obtained in these four channels, which correspond to different temperatures. The 195 Å EIT filtergrams were used to detect and analyze the coronal disturbance propagating over the disk and above the limb in the given event. These disturbances manifest themselves in the Yohkoh/SXT soft X-ray images [42], which correspond to temperatures exceeding 2.5 MK. The characteristics of the large-scale CME associated with the event considered here were studied using data from the SOHO/LASCO white-light coronograph at heliocentric distances from 2.5 to $32R_\odot$ [43].

The EIT and LASCO input data files are accessible at the sites http:/umbra.nascom.nasa.gov/eit/eit-catalog.html and http:/lasco-www.nrl.navy.mil/cgi-bin/lwdb/lasco/images/form. The routine processing of the SOHO/EIT images was carried out using the procedure "eit_prep" (J. Newmark). We carried out the preliminary reduction of the Yohkoh/SXT telemetry data using the procedure "sxt_prep" (M. Morrison) and the required Yohkoh database.

The main reason that large-scale disturbances associated with eruptions have been relatively poorly studied is their low contrast, which makes them difficult to distinguish in images that have not been subject to specialized processing. For this purpose, we used difference images with a fixed frame before the event subtracted, with a preliminary compensation for the solar rotation in all images (see, for example, [6, 7]). To distinguish rapid variations (such as "EIT waves"), we used the running difference images formed by subtracting the previous frame from each image. We also used the unsubtracted images subjected to deep contrast enhancement.

We also used fixed-base difference images to analyze the CME using the LASCO data, but without compensation for the solar rotation. These enabled us to trace the development of the CME in the plane of the sky compared to the pre-eruption image of the corona. Due to the limited space available in this article, we present here only the most important illustrations. Additional images and films illustrating the development of the event are available at the site http:/helios.izmiran.troitsk.ru/lars/Chertok/990912/index.html.

3. ERUPTION OF THE Hα FILAMENT

The analyzed Hα filament 1-2 (Fig. 1a) was part of the eastern branch of an extended U-shaped filament that occupied an appreciable region in the southwestern quadrant of the solar disk. Substantial variations of the northern end of the large filament 3 were observed for several hours before the eruption; a gradual decay of the intermediate part of filament 2-3 [frames (b) and (c)] began after ≈22 : 15[1] on September 11. This decay did not display any signs of an eruption, and was most likely due to heating of this part of the filament.

The first manifestations of the impending destabilization of the central part of the filament 1-2 are variations of its contrast, clearly visible on a film, which resemble disturbances traveling along the filament. Starting from ≈23:00, there was a gradual splitting off of the western component (thread) of the filament 1-2 from the initial position of the main filament and a slow shift of this component toward the southwest [frame (d)]. At this stage, over a few tens of minutes, the splitted-off component moved a large distance in the sky plane, comparable to the visible width of the filament. More distinct and rapid eruptive phenomena were observed after ≈23:55, when first several small northern fragments of the filament 1-2, and then the entire filament, began to be torn off and move appreciably toward the west/northwest. The arrow in frame (e) marks the position of one of the eruptive fragments of the filament at 00:03:14 on September 12. The available filterframs allow us to trace the motion of this fragment until ≈00:15, when it had moved 45 000 km relative to its pre-eruptive position. An analysis of the kinematics of these fragments, the eruptive structures in the EUV, and components of the CME is presented in Section 6. By 00:20–00:21, this process had led to the nearly complete disappearance of both the main filament 1-2 and its continuation to the northern end 3 [frame (f)], where substantial motion of the western filament branch was also observed. The filament component 4 located further to the north was not part of the U-shaped filament considered, and corresponded to another structure located near the polarity-reversal line of the magnetic field. However, this component was also affected by disturbances from the erupted filament 1-2-3: and a flow of dark material in this filament was observed in the Hα and 195 Å channels long after the eruption.

In the next phase, two main features were observed in Hα, whose development is illustrated by frames (g)–(i) in Fig. 1. First, beginning at 00:24, the glowing flare-like ribbons aa and bb appeared on either side of the erupting northern part of the filament 1-2. As in eruptive flares, these ribbons gradually became elongated along the filament, mainly toward the south, and diverged appreciably in the transverse direction. Over 50 min, the distance between them increased from 35 000 to 60 000 km. In spite of the large dimensions of these ribbons, their brightness was modest, and this event was not classified as an optical flare. Second, diffuse brightenings were observed simultaneous with the development of the ribbons [arrows in frames (g) and (h)]. One of these appeared at about 00:22 to the northwest of position 1, and then moved ≈220 000 km to the southeast along the southern component of the filament 1-5 with a mean speed of ≈145 km/s (this brightening was also detected in radio images synthesized from data of the Nobeyama Radio Heliograph at 17 GHz with one-minute averaging, which indicates enhanced temperatures in this region). Further, the contrast was increased, and the southern component of the filament 1-5 broadened and moved to the southwest [frame

[1] All indicated times are UT.

(i)]. At 00:27–00:30, we can also note a barely detectable brightening that moved from position 3 to the north/northeast, towards an AR. After 00:50, the southeastern part of the filament structure begins to become restored, but has shifted to the southwest of its pre-eruption position. The Big Bear observations ended at 01:18.

The phenomena considered here can fit into the following general picture for the eruption of the Hα filament. The main onset of the eruption occurred in the central zone of the filament 1-2, and during its rise the northern (2-3) and southern (1-5) extended branches of the filament were involved in the eruption. The extended filament structure took the form of a bell cross section, with its upper part pulled upward and fixed southeastern and northwestern ends. As it was stretched, some part of the heated plasma flowed downward to the ends of the structure (most toward the southeastern end), then cooled.

4. DIMMINGS

The EUV and soft X-ray images obtained with SOHO/EIT and Yohkoh/SXT provide additional information about the filament eruption and the accompanying large-scale phenomena. Figure 2 shows the images obtained in the four 304, 171, 195, 284 Å SOHO/EIT channels (four upper rows) and the Yohkoh/SXT image (lower row) in order of increasing temperature from top to bottom. The left and right columns show the corresponding unsubtracted images obtained before and ≈ 6 h after the eruption. The two middle columns present the fixed-base difference images near the maximum of the event (01 UT) and in the late post-eruptive stage (07 UT).

The difference images [Fig. 2, from frames (f)–(j) to frames (k)–(o)] show the development of large-scale, long-lived dimmings [dark regions marked in frame (g)] and an extended, emitting post-eruptive arcade and its associated flare-like ribbons. As is true of many other eruptive events, the two dimmings D1 and D2 are located on either side of the arcade; i.e., of the filament and magnetic polarity inversion line. This is in agreement with the standard picture, in which the dimmings D1 and D2 are located at the bases of an erupted magnetic rope structure associated with the filament. We can also note two more large, removed dimmings: the northeastern dimming D3 and southwestern dimming D4. The original and difference images in Fig. 2 show that the southeastern (D1) and northeastern (D3) dimmings are connected by a system of large-scale loops. Many of these loops also appear dark in the difference images, and the dimmings D1 and D3 are located in the fields of negative and positive polarity, respectively. It follows that not only magnetic structures located above the filament and rooted in the dimmings D1 and D2 participated in the eruption, but also the large-scale systems of loops connecting the dimmings D1 and D3.

The manifestation of dimmings and other long-lived phenomena in channels corresponding to various temperatures is demonstrated by the difference images presented in the two middle columns of Fig. 2. Frames (f)–(j) and (k)–(o) display large-scale disturbances approximately 1 h and 7 h after the filament eruption, respectively. The dimmings D1 and D2 adjacent to the filament over several hours appear similar in the 171, 195 and 284 Å coronal channels, and somewhat weaker in the 304 Å channel [at about 01 UT, frame (f)]. The dimming D3 is barely distinguishable in this channel, only in the frame near 07 UT [frame (k)]. The dimming D4 is similar in all the channels, with its outline changing slightly from frame to frame. A more complete set of unsubtracted frames in the 195 Å channel shows that the darkening in this region is due to the variable northern filament 4, which is also visible in Hα (Fig. 1).

The Yohkoh/SXT soft X-ray images (Figs. 2j, 2o) also show regions of reduced brightness near D1 and D2 that are similar to those observed in the EUV lines. With time, the developed post-eruptive arcade expanded in the region of these dimmings, reducing their area. Similar behavior is observed in the eastern part of D1. The expansion of the arcade in the soft X-rays leads the narrowing of the dimmings in the EUV, which corresponds to cooling of the loops in the standard picture.

The situation near and to the east of D3 seems unusual: the darkening in the EUV corresponds to a brightening in the soft X-rays (Figs. 2h, 2j). This brightening is modest, but clearly visible. The heights of structures emitting in the EUV before the eruption (i.e., dimmings) and in the soft X-rays after the eruption could be substantially different, and their apparent spatial coincidence could be a projection effect. However, there are no appreciable brightenings in any of the EUV channels, even near D3. Consequently, the phenomenon observed near D3 can be explained only by heating of the plasma above 2.5 MK, as a result of which its radiation lies outside the range of temperature sensitivity of the EIT channels, but it remains visible in the soft X-ray.

There was a break in the Yohkoh/SXT observations from 00:58:56 to 01:43:44. After this break, no brightening is observed near and to the East of D3, but D3, D4, and D2 have merged into a single dark region that slowly expanded toward the north until 04:00 on September 12. This region resembles a coronal hole (CH) in the soft X-rays, and subsequent variations are not observed in it. Our analyzed

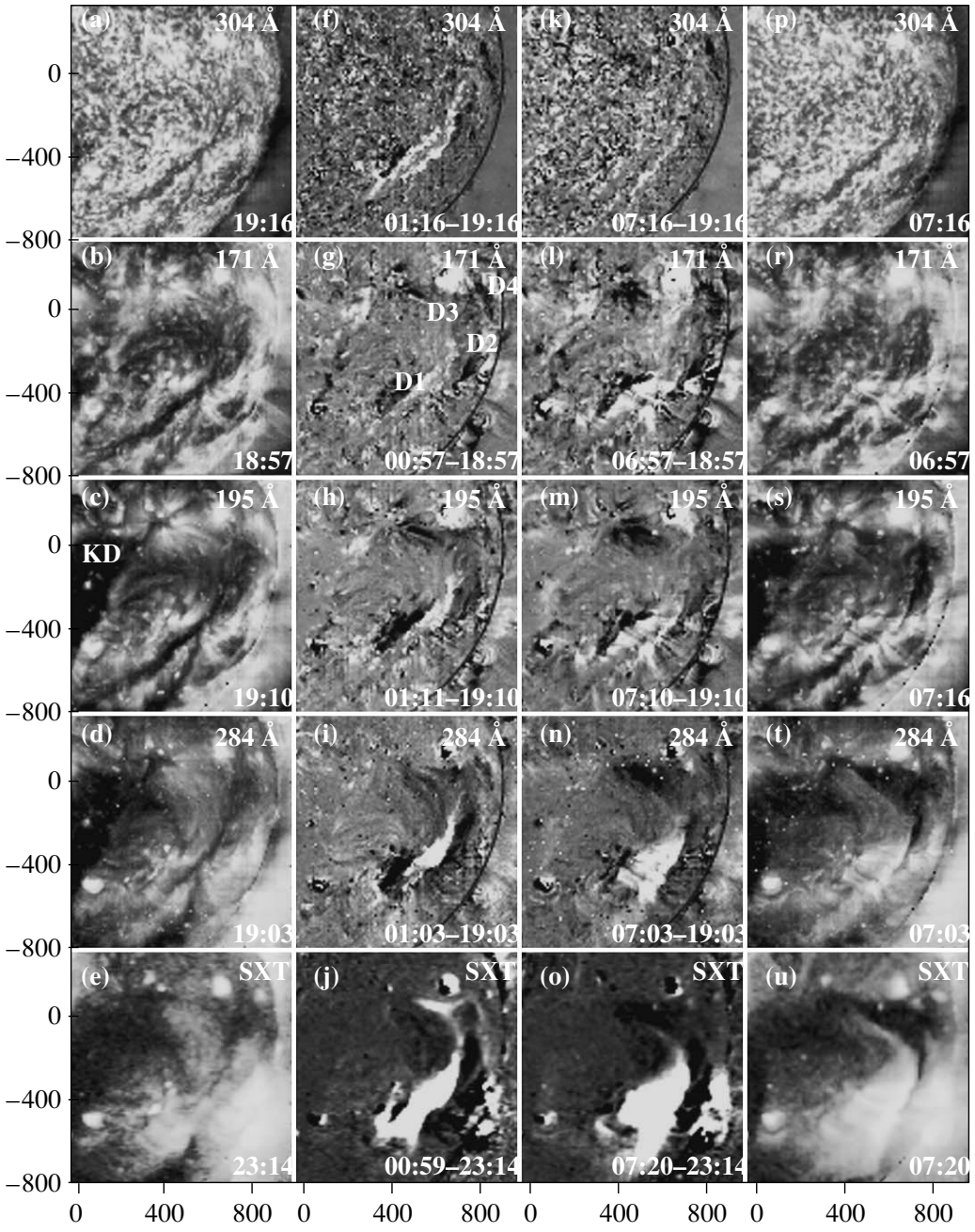

Fig. 2. Images in the SOHO/EIT 304, 171, 195, 284 Å (four upper rows) and Yohkoh/SXT (lower row) channels. The left and right columns show the corresponding unsubtracted images before and ≈6 hr after the eruption of the filament. The two middle columns show the fixed-base difference images at times of about 01^h and 07^h UT.

Yohkoh/SXT data end on September 12 at 10:11. Note that, before the event, part of the area of this future CH was occupied by soft X-ray loops (Fig. 2e). As we have indicated, no such large hole was observed in the EIT coronal channels; the appreciably smaller-area dimmings D2, D3, and D4 separated by emitting structures continue to be present at least until 07:00 on September 12. The existence of dimmings in both the EUV and soft X-rays cannot be explained as a result of temperature variations. Consequently, a lowering of the plasma density in these regions began at 00:59–01:44, apparently due to its outflow into open coronal structures.

Information about the degree of brightness reduction (depth) of the dimmings in the 195 Å channel and their evolution is presented in Fig. 3. The temporal

profiles of the brightnesses in various places in each dimming are not the same; we show here typical temporal profiles in the four 10 × 10-pixel areas marked in frame (a) in the dimmings D1–D4 and in two places in the central part of the CH adjoining to the eastern boundary of the eruption region. The temporal profiles in dimmings D1, D2, and D3 are generally identical. The western dimming D2 began its development earlier than the others, at 23:57–00:09, in the stage when the filament was slowly shifting its position. The reduction of the brightness in the eastern (D1) and northeastern (D3) dimmings began abruptly between 00:09 and 00:21, roughly coincident with the beginning of the phase of rapid eruption of the filament. In some places, in particular in the dimming D1, we can note a slow lowering of the brightness even in the pre-eruptive phase, starting from ≈22:33 on September 11. The reduction time of the brightness in dimmings D1–D3 is one to two hours. The brightness reduction in the dimmings does not reach the level of the eastern CH, in whose central area (CH1) the low brightness remains virtually constant over the entire studied time interval. The brightness in the CH region marked CH2 non-monotonically grows with time; this is discussed in Section 6. The maximum relative depth of dimming D1 reaches 75%, and the depths of D2 and D3 are 60–65%. As the measurements near 01:00 show, the depths of D1 and D2 are also appreciable in the 304, 171, and 284 Å channels—50–70%. The brightness variations in the absorption-induced dimming D4 due to motions of the filament differ from those for D1–D3, and its depth does not exceed 35%.

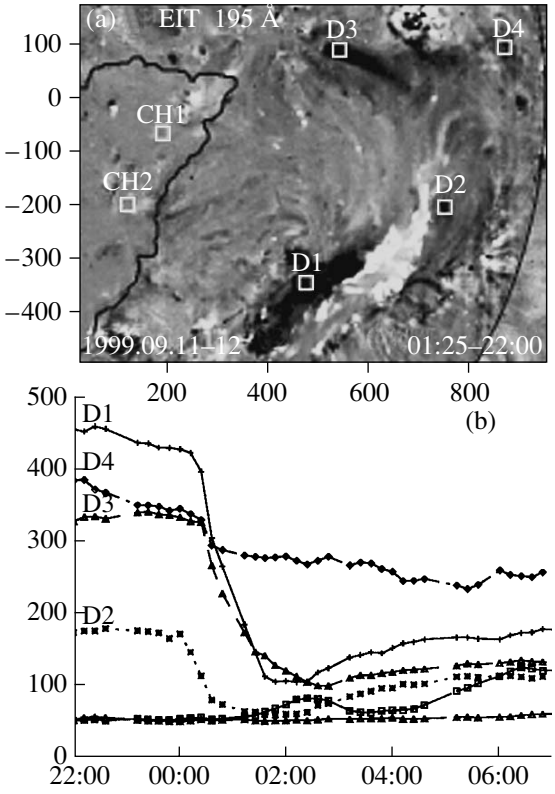

Fig. 3. Temporal profiles (b) of the dimmings D1, D2, D3, and D4 in the 10 × 10-pixel areas marked in the upper part of frame (a) in the 195 Å channel. For comparison, we also show the brightnesses in two areas of nearby coronal holes, which are nearly constant in CH1 and non-monotonically increasing in CH2. The dark contour corresponds to the boundary of the coronal hole.

5. PHENOMENA ALONG THE MAIN NEUTRAL LINE

In contrast to eruptive flares in ARs, where the main neutral line can usually be clearly traced, the chaotic pattern of intermittent small-scale weak fields of different polarities we are dealing with here hinders identification of the neutral line. Nevertheless, the run of this line can be deduced in several ways. First, for both September 11 and September 12, all 15 SOHO/MDI magnetograms of the full disk obtained over a full day of observations were reduced to a single time, compensating for the solar rotation, and then averaged. These averaged magnetograms were then subject to deep smoothing, which suppresses fluctuations and rapid magnetic-field variations, allowing us to understand the approximation run of the main neutral line. Second, magnetic-field maps for 23:20 on September 11 calculated from the Stanford Observatory synoptic maps using the program of V.N. Obridko et al. and extrapolated in a potential approximation for heights of $(0.1–0.2)R_\odot$ show a similar result. The results obtained in both ways correspond to the position of the Hα filament and its elements along the line 1-2-3 (Fig. 1a), as well as their continuation to the southeast.

As we have noted, the depth and area of the dimmings gradually decreased in the late post-eruptive phase (Figs. 2, 3; especially D1 and D2), in particular, due to the fact that the post-eruptive arcade and its well defined, flare-like ribbons developed along the main neutral line simultaneously with the dimmings, increasing their length and width with time. Short ribbons appear at 00:21 in the 195 Å channel, to the sides of the erupted filament 1-2 (Fig. 4b). These are similar to the Hα ribbons visible at the same time (Fig. 1g). The distance between them at that time was 43 000 km. Further, the development of the arcade and loops rooted in the ribbon kernels is observed in the coronal channels. The extent of the arcade and ribbons to the north and south increases with time, and the ribbons move apart (the transverse size of the arcade grows). This corresponds to the formation of increasingly higher loops in the post-eruptive stage. The ribbons are most clearly visible in the 304 Å

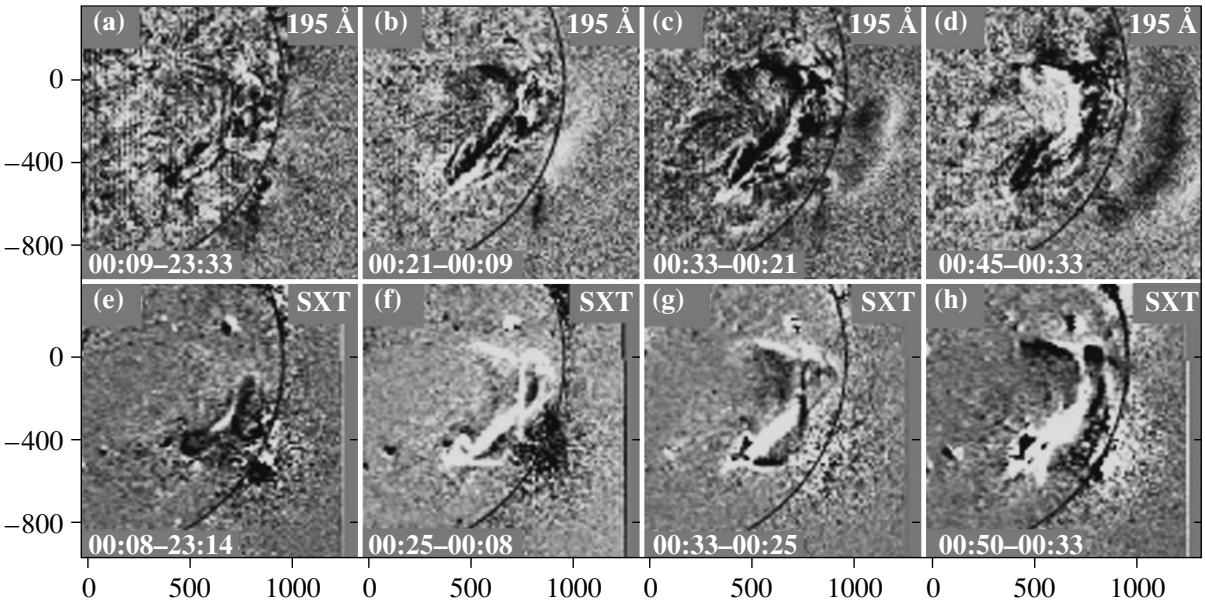

Fig. 4. Running difference images of SOHO/EIT in the 195 Å channel (a)–(d) and in soft X-rays from Yohkoh/SXT data (e)–(h) illustrating the coronal disturbance ("EIT wave"), which was quasi-stationary on the disk and propagated above the limb.

channel (Figs. 2f, 2k). The north–south extent of the ribbons in this channel had grown to ≈525 000 km ($0.75R_\odot$) by 01:16; the maximum distance between the ribbons had grown to ≈140 000 km ($0.2R_\odot$) by 07:19. The bright arcade is clearly defined in its central region, near the positions 1-2, where the photospheric magnetic fields reached several hundreds of Gauss. The magnetic fields further from this region did not exceed 100 G, and alternated with the fields of opposite polarity. The distance between the ribbons to the northwest decreased as they appeared to converge. These ribbons were broader than flare ribbons, and displayed fine structure determined by the photospheric magnetic fields. Note that these features are typical for filament eruptions outside ARs.

The Yohkoh/SXT soft X-ray arcade (Figs. 2j, 2o, 2u) displayed approximately the same character and parameters as the arcade in the EIT 195 and 284 Å coronal channels (Figs. 2h, 2m, 2s and 2j, 2n, 2t). In spite of the appreciable dimensions and substantial apparent brightness of the post-eruptive arcade in both the EUV and soft X-ray ranges, its contribution to the total solar radiation flux was insignificant: the X-ray monitors on the GOES satellite indicate that the 1–8 Å flux from the arcade was close to the noise level, and did not exceed B5, i.e., 5×10^{-7} W/m^2.

Another feature detected along the main neutral line in the unsubtracted 195 Å EIT images is a narrow, extended brightening that propagated from the region 1-2 toward the north at 00:21–00:33 and toward the southeast at 00:33–01:11 (it is barely discernible in Figs. 4b–4d). The southeastern component has a filamentary structure. This brightening is also visible in the soft X-rays, where the southeastern component is seen to lie below the forming flare loops. The times and locations of these brightenings and the directions in which they propagated are consistent with those for similar features observed in Hα in the main eruptive phase, associated with heating of the plasma and its outflow from the center of the eruption (the region 1-2), along the filament axis. This most likely represents a brightening of rising parts of the filament that remained at the solar surface after the eruption. Similar phenomena are fairly frequently visible on TRACE films. The filament became bright in the 195 Å channel only when it was heated, and the propagation of the region of brightening could be related to both motion of the region of heating (with a wave-like character) and the flow of plasma along the filament.

6. THE PROPAGATING CORONAL DISTURBANCE AND CME

It is not only structures directly participating in the eruption that are subject to disturbances initiated by the eruption. Coronal disturbances can propagate to large distances in all directions. They can be traced via the brightness variations in the images in the EUV and other wavelength ranges. In addition

to regions of decreased brightness, regions displaying large-scale, weak brightening are also observed, which have obtained the name "EIT waves." These are observed both in flare eruptive events and in some filament eruptions outside ARs [12, 44]. In the event analyzed here, such a disturbance is visible in the EIT 195 Å difference images. The favorable location of the eruption center near S20 W45 made it possible to observe this feature both on the disk and above the limb. Figure 4 presents relative running difference EIT images (divided by the pre-eruption image for 23:33) and Yohkoh/SXT data. All the images were subject to a non-linear processing designed to reveal coronal disturbances with very low brightnesses.

A very weak oval-shaped brightening can be seen in frame (b) (September 12 at 00:21). The fragmentary brightenings in its eastern part are located approximately at the western boundary of a nearby CH, where dark dimming loops (i.e., loops with reduced brightness) emerging from the vicinity of the erupting filament (the dimming D1) are also rooted. The fragmentary disturbance in the southern part of the oval are identified with a brightening front, which, like the Hα brightening (see Section 3), propagated to the southeast along the southern part of the filament in this stage. The northern sector of the disturbance approximately coincides with the northern end of the pre-eruption filament and the region where the northern part of the dimming D3 developed. The western sector of the disturbance has an arc-like shape that rises to heights of 70 000 km above the limb in the plane of the sky. In subsequent images, the position of the southern, eastern, and northern sectors of the coronal disturbance vary only insignificantly. In the eastern part of the southern sector, near the southern end of the filament, the disturbance moved slightly (by 40 000 km), in agreement with the continuing propagation of the southeastern brightening. The position of the eastern sector near the western boundary of the CH was nearly constant, as is often observed in flare events [3, 45]. At the same time, the western arc above the limb and its southern continuation on the disk, which can be seen in the frame for 00:33, rapidly expanded. The height of the western arc had reached 330 000 km by 00:45 [frame (d)]. The results of our analysis of the kinematics and properties of this structure and a comparison with the kinematics and structure of the CME are presented below.

The coronal disturbance was also manifest in Yohkoh/SXT soft X-ray images (Figs. 4e–4h). The eastern (on the disk) and western (at the limb) components of the disturbance have a diffuse character. As in the EIT 195 Å channel, the eastern component is contained by the western boundary of the nearby CH, while the western component resembles an extensive, amorphous brightening above the limb.

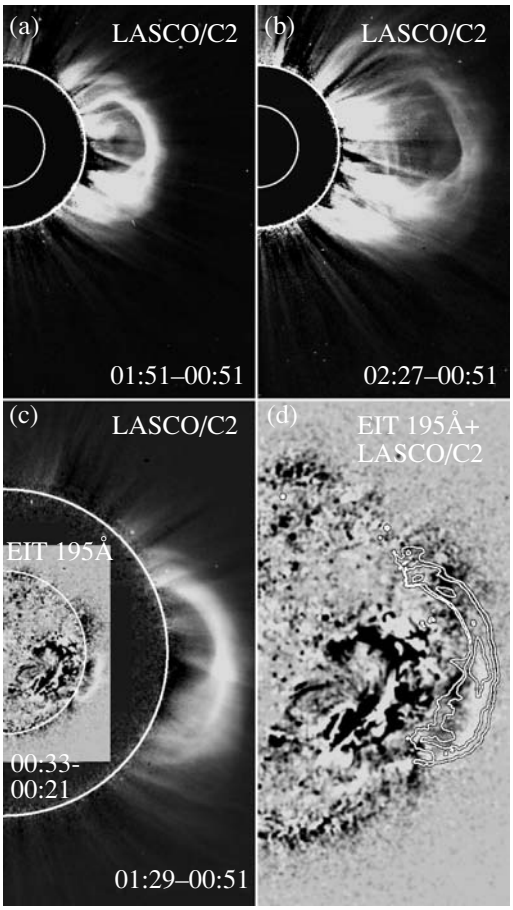

Fig. 5. (a, b) Fixed-base difference images of the CME constructed from the SOHO/LASCO/C2 data. (c, d) Running difference EIT 195 Å and LASCO/C2 images shown on a single scale, together with a contour showing the frontal structure of the CME and an image of the rising UV arc, demonstrating the self-similarity of these formations.

The northern brightening considered in Section 4 moved slowly to the north towards the AR, but did not reach it. The lengthening toward the southeast is similar to the moving brightening observed in Hα and the 195 Å channel. The eruption of the large-scale, hot structure can clearly be traced in frames (e), (f), and (g).

The eruption considered led to the formation of a CME that is visible in LASCO/C2 fixed-base difference images obtained in white light (Figs. 5a, 5b). The CME had a front structure in the form of a large structured loop encompassing position angles from 220° in the south to 320° in the north. The central part of the filament 1-2 and the direction of the eruption of its fragments in Hα (Fig. 1) and the EIT 195 Å channel (Figs. 2 and 4) are close to the position of the southern "leg" of the loop-like CME. Two bright components can be distinguished in the CME, whose

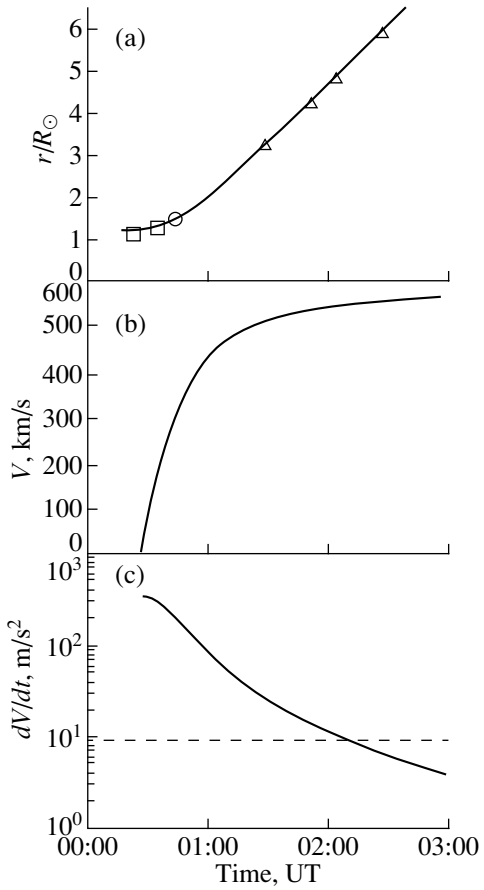

Fig. 6. (a) Distance from the disk center of the rising arc $r/R_\odot$ in the three EIT filtergrams in the 195 Å channel (squares and circle), the position of the CME front in the four LASCO/C2 images (triangles), and a calculated plot of the self-similar expansion of the CME. (b,c) Plots of the calculated velocity V and acceleration dV/dt.

frontal parts are joined with the inner structure of the CME by thin, weak emitting radial elements. The similarity of the position angles and overall character of the observed structures suggests that the erupting filament fragments can be identified with these two components of the southern "leg" of the CME. The central and northern components of the CME front probably correspond to erupted large-scale loops that are associated with the dimmings D1 and D2, as well as D1 and D3 (see, for example, Figs. 2h, 2i and Fig. 4f).

What is the nature of the arc of coronal disturbance expanding above the western limb observed in the 195 Å channel (Fig. 4a–4d), and how is it related to the frontal loop of the CME? Figure 5c shows the clearest image of this arc at 00:33 and the first image of the CME at 01:29 together on the same scale. In spite of the nearly hour difference in time, the similarity in the positions, shapes and structural details of the arc of the "EIT wave" and the frontal loop of the CME is striking. In particular, a bright triangular feature can be distinguished in the central zones of both the arc and the loop, with the widths of both structures decreasing abruptly to the south of this feature. In contrast to the CME loop, the northern part of the arc is not detected in the 195 Å channel, presumably because its temperature differs substantially from those to which this EIT channel is sensitive. The similarity of these two structures is demonstrated by their superposed images shown on the same scale (Fig. 5d; the scaling coefficient can be found from Fig. 6a). This coincidence in the presence of the different physical sizes of these structures and the appreciable difference in the observing times leads to two important conclusions. First, the arc observed above the limb in the EUV and the frontal structure of the CME represent the same objects. Second, the motion of this object is self-similar; i.e., it retains the same appearance as it expands with time.

These conclusions are supported by a kinematic analysis similar to that presented in [12]. We constructed two similar ovals from the geometric center of the expanding arc passing through the parts of the "EIT wave" that are detected in the 195 Å channel. The measured distances from the center of the solar disk to these ovals at a position angle of about 270°, approximately along the radial axis of the "EIT wave", are presented in Fig. 6a. These distances correspond to the observed positions of the leading edge of the "EIT wave" in the plane of the sky at 00:21 and 00:33 (squares in Fig. 6a), as well as at 00:45, when the leading edge of the arc left the field of view; the distance was estimated in this way using the lateral parts of the arc (circle in Fig. 6a). The triangles present the positions of the CME front in the four LASCO/C2 images from the SOHO LASCO CME Catalog (http:/cdaw.gsfc.nasa.gov/CME_list/). A fit curve for the self-similar expansion of the CME [12] passing through all these points corresponds to the following initial parameters: velocity of 0.1 km/s, onset of the self-similar expansion of 00:19:00, and initial size of the expanding structure of 500 000 km. The asymptotic velocity of the CME front (at a large distance from the Sun) was 595 km/s (Fig. 6b), somewhat lower than the estimate obtained in the CME catalog based on a linear approximation of the LASCO data (732 km/s). This latter speed was determined in the CME catalog for several different position angles using the fastest feature in the CME, at its leading edge. The parameters we have found are in good agreement with the observations. The initial size of the self-similarly expanding structure, 500 000 km, is close to the observed scale of the eruption, characterized, for example, by the extent of the flare-like ribbons visible in the EIT 304 Å channel

in Fig. 2f [12]. The derived onset of the self-similar expansion (00:19:00) is close to the time of the first manifestations of the large-scale coronal disturbance in the EIT and Yohkoh/SXT frames (Fig. 4). Recall that the slow ascent of the structures before the eruption (with small or no acceleration) was not self-similar, and is not fit well by our solution for the expansion. Moreover, our derived onset time is more realistic than the extrapolated time for the onset of the CME based on a polynomial fit to the data in the CME catalog (no earlier than 00:48).

Figures 6b, 6c show the corresponding plots of the velocity and acceleration of the CME obtained by differentiating the calculated curve presented in Fig. 6a. Note that the calculated curve is in full agreement with the experimental points, and the character of the corresponding velocity variations is fundamentally different from the parabolic relation assumed in the second-order polynomial approximation of the catalog data. The acceleration of the CME, which was initially about 350 m/s^2, decreases by two orders of magnitude in the three-hour interval considered. For comparison, the dashed line shows the acceleration presented in the CME catalog (9.2 m/s^2).

Another interesting phenomenon was observed in the western part of the CH, most clearly visible in the high-contrast, unsubtracted EIT 195 Å images (Figs. 2c–2e and 2s–2u). The eastern roots of the long loops going out from the eruption region lie approximately half-way between the largest coronal bright point at the center of the CH and the western boundary of the CH. These ends brightened appreciably at 00:45, and a number of subsequent frames (to 02:00) show that the loops initially emerging at a small angle to the surface "straighten themselves up," so that their "legs" become nearly vertical; i.e., the magnetic field becomes more radial. Still later, beginning at 03:33, a number of low, closed loops appear to the north of this region, which are clearly visible beginning at 05:33 (Fig. 2m). These phenomena are reflected by the variations in the brightness of the region CH2 in Fig. 3b.

7. DISCUSSION AND CONCLUSION

The event of September 12, 1999 demonstrates that large-scale disturbances accompanying the eruption of a filament outside an AR are no less spectacular than those in flare events. In many ways, the phenomena accompanying filament eruption are similar to their analogs observed in flares. Although the filament eruption occurs in relatively weak magnetic fields, it is probable that the same eruptive and post-eruptive processes occur as those in CMEs associated with flares in ARs, which determine their overall properties. However, there are also differences between the two, caused first of all to the character and strength of the photospheric magnetic fields below the eruption region. The magnetic fields in events outside ARs are weak, and the opposite polarities alternate in a chaotic fashion on small scales.

At the beginning of September 12, after the slow, pre-eruptive ascent, the Gaussian-like filament structure formed by the elements 1-2 and its apex became elongated at a rapidly increasing rate. Overall, the phenomena in the central part of the region involved in the eruption are consistent with the standard flare model ("CSHKP") and current concepts based on observations of other eruptive events. The photospheric magnetic fields in this region were fairly strong, to several hundreds of Gauss, which determined the location of the brightest sections of the ribbons.

The elongation ("opening") of the transverse loops encompassing the long filament structure from above was accompanied by magnetic reconnection below the receding filament, in accordance with the standard model. The energy release resulted in substantial heating in this region (>2.5 MK according to the Yohkoh/SXT data). The plasma density in the loops decreased appreciably as they opened, leading to the formation of the dimmings D1 and D2 to the sides of the arcade. The brightness in these regions was also reduced in the EUV and soft X-ray ranges; consequently, this was due to an outflow of plasma, but not temperature effects [3, 6, 11]. Note that the measured reduction in the emission measure by 75% corresponds to a decrease in the plasma density by a factor of two.

It is reasonable to expect the appearance of dimmings at the ends of the long magnetic structure—the Hα filament and associated hotter structures — as it is stretched out (note that D1 and D2 occupy an intermediate position between the sides and ends of the arcade). However, in this event (as in many others), a spreading of the cooled plasma from the central heated region of the spine of the arcade toward the edges of the elongated erupted magnetic structure was observed, as is demonstrated by the Hα, EUV, and X-ray data. The simultaneous appearance of flows in all these wavelength ranges testifies to a broad range of temperatures in the spreading plasma, from 10^4 K to >2.5 MK. The flows along those parts of the filament remaining near the solar surface that were clearly observed in this event distinguish it from a situation in which there is a phase shift in the observed brightenings due to motion of the region of energy release, with successive magnetic reconnection below those parts of the filament that are involved in the eruption [36].

In addition to these flows, there is evidence for "sliding" of the loops encompassing the long filament structure near its ends before the eruption. These loops should "slide" closer to its ends as the erupting structure is elongated. As a result, the mean plasma density in the regions of these ends should grow, giving rise to brightening, as was indeed observed near the southeastern end of the filament structure, where the flow of plasma was most clearly visible. Recall that the presence of such brightenings in the EUV, e.g. in the 195 Å channel, testifies to an enhancement of the density of plasma with the normal coronal temperature, rather than to an increase in the temperature of this plasma.

The dimming D4, as indicated, was due to absorption in the active filament; similar phenomena have been observed earlier [13]. The phenomena in the region of the dimming D3 testify to a different situation. The soft X-ray brightening that shifted slightly to the north (Figs. 4f, 4g, 4h) indicates magnetic structures compressed from the south as a result of the eruption; these structures were heated to temperatures exceeding 2.5 MK, by a mechanism whose nature is not clear. This was followed by an evacuation of plasma from this region, as well as from the regions of D1 and D2, bringing the pictures observed in the EUV and X-ray into agreement with each other (Figs. 2m, 2n, 2o). Temperature variations during the formation of some dimmings have been noted earlier based on spectral observations [46].

The eruption of structures between D1 and D2 is directly demonstrated by various observations, but an eruption also clearly occurred at the continuation of the long arc to D3 as well. This is indicated by the appearance of the dimming D3, the presence of the northern loop of the CME, and the phenomena observed in the soft X-ray range (Figs. 4f, 4g). However, while the filament and the above-lying structures were ejected in the region between D1 and D2, the higher (and hotter) structures located to the north of D2, and probably further to D3, erupted, whereas lower structures (and probably the filament itself) remained at the solar surface, at least in the first stage of the event. It is not clear whether the magnetic structure from D1 to D3 erupted as a whole, or whether an initial eruption between D1 and D2 led to a subsequent eruption right to the location of D3. The unified CME structure with its similar southern and northern branches, the virtually simultaneous onset of the brightness reduction in the dimmings D1 and D3, and the shape of the expanding ejection in the Yohkoh/SXT difference images at 00:16–00:33 (Figs. 4f, 4g) all support the idea that the entire magnetic structure erupted essentially simultaneously. In this case, the presence of the dimming D2 and the fact that its development overtook that of the other dimmings looks like a merging of filaments in a two-segment model for the initiation of a CME [47].

As in the case of flares, the formation of a post-eruptive arcade and extended flare-like ribbons at its roots was observed. These ribbons were broader than flare ribbons and had structures in accordance with the associated photospheric magnetic fields; this also determines the appearance of the above-lying loops. Moving along the main neutral line in the region of weaker fields, we find less bright ribbons and loops. The transverse dimensions of the arcade several hours after the eruption reached 140 000 km, with the maximum extent of the ribbons reaching 520 000 km. In spite of their substantial dimensions and brightness, their total radiation flux was much less than that observed during eruptions in ARs, which are characterized by arcades and ribbons that are much smaller but brighter [33, 48]. In both types of events, primary thermal processes are observed in the corona, but, in eruptions outside ARs, there are no visible manifestations of particle acceleration, which determine the powerful processes characteristic of the impulsive phases of flares. In this connection, the eruption of filaments outside ARs, including the event considered here, differ from flare eruptions occurring in the strong magnetic fields of ARs.

The observational data and our kinematic analysis suggest the following interpretation for the "EIT wave" observed in this event. The western arc of the "EIT wave" above the limb (and its southern continuation on the solar disk) mark the frontal structure of a CME in an early stage of self-similar expansion. This is probably typical for filament eruptions outside ARs, since the formation of shocks during the prolonged, smooth acceleration of the ejection starting from low initial speeds is unlikely, and the object expanding above the limb can only be a stretched magnetic structure. On the contrary, the propagating coronal disturbances in sufficiently powerful flares could be manifestations of explosive shocks [13, 28, 30].

The quasi-stationary eastern and northern oval sectors on the disk in the region of the western boundary of the CH and in the north, near the boundaries of other magnetic domains (separatrices) associated with an active region lying further to the north, may represent contours of coronal structures associated with the "base" of the expanding CME. The brightening in the EUV is caused by an increase of the mean plasma density due to the compression of coronal structures. In the simplest picture, the propagating coronal disturbance stops at the boundary of the CH, whose magnetic field is supposed to be radial; the further propagation of the disturbance is hindered by the boundaries between different magnetic domains [3, 45]. The general features of this scenario are confirmed, but the observations also suggest a more

complex picture. The magnetic field in the CH is appreciably non-uniform; moreover, long loops emerging at small angles into the zone of the CH are present before the eruption. These loops are transformed during the course of the events, with the field in the parts entering the CH becoming more radial, after which closed, low-lying loops form in this region of the CH, leading to the disappearance of this part of the CH (compare Figs. 2c, 2d, 2e and Figs. 2s, 2t, 2u). In this respect, this brings to mind an event with a filament eruption inside a CH [49].

The expansion of the erupted structures visible near the solar surface and the CME observed by the LASCO/C2 coronograph is self-similar, i.e., it preserves the shape of these structures. A self-similar expansion provides a better description of the kinematics of the ejection than the polynomial approximation used previously, based on an assumption of constant or zero acceleration. It is important that the initial expansion of the CME is characterized by appreciable acceleration, which then rapidly decreases with time. This is the cause of the incorrectness of conclusions based on polynomial approximations and the inconsistencies displayed by a number of studies, for example, between the times of eruptions and the onsets of the associated CMEs.

ACKNOWLEDGMENTS

The authors thank the SOHO/EIT, SOHO/LASCO, and Yohkoh/SXT teams for the data used in this analysis (SOHO is an international collaboration between ESA and NASA; Yohkoh is a mission led by a number of institutes in Japan, the USA, and the United Kingdom). We also thank V. Yurchishin for the Big Bear Observatory Hα filtergrams. This work was supported by the Russian Foundation for Basic Research (project codes 06-02-16106, 07-02-00101, 09-02-00115, 09-02-00544), the Minister of Education and Science of the Russian Federation (grant NSh-4573.2008.2), and the Basic Research Programs of the Russian Academy of Sciences "Plasma Heliophysics" and "Solar Activity and Physical Processes in the Sun–Earth System."

REFERENCES

1. *Coronal Mass Ejections*, Ed. by H. Kunow, N. U. Crooker, J. A. Linker, et al., Space Sciences Ser. of ISSI **21** (2006); reprinted from Space Sci. Rev. **123** (2006).
2. B. P. Filippov, *Eruptive Processes on the Sun* (Fizmatlit, Moscow, 2007) [in Russian].
3. B. J. Thompson, S. P. Plunkett, J. B. Gurman, et al., Geophys. Res. Lett. **25**, 2465 (1998).
4. D. F. Webb, J. Atmosph. Solar-Terr. Phys. **62**, 1415 (2000).
5. H. S. Hudson and E. W. Cliver, J. Geophys. Res. **106**, 25199 (2001).
6. I. M. Chertok and V. V. Grechnev, Astron. Zh. **80**, 162 (2003) [Astron. Rep. **47**, 139 (2003)].
7. I. M. Chertok and V. V. Grechnev, Solar Phys. **229**, 95 (2005).
8. Y. Zhang, J. Wang, G. Attrill, et al., Solar Phys. **241**, 329 (2007).
9. A. A. Reinard and D. A. Biesecker, Astrophys. J. **674**, 576 (2008).
10. L. K. Harra and A. C. Sterling, Astrophys. J. **561**, L215 (2001).
11. L. K. Harra, H. Hara, S. Imada, et al., Publ. Astron. Soc. Japan **59**, S801 (2007).
12. A. M. Uralov, V. V. Grechnev, and H. S. Hudson, J. Geophys. Res. **110**, A05 104 (2005).
13. V. V. Grechnev, A. M. Uralov, V. A. Slemzin, et al., Solar Phys. **252**, 149 (2008).
14. G. E. Moreton and H. E. Ramsey, Publ. Astron. Soc. Pacif. **72**, 357 (1960).
15. H. R. Gilbert, T. E. Holzer, B. J. Thompson, and J. T. Burkepile, Astrophys. J. **607**, 540 (2004).
16. C. Delannée and G. Aulanier, Solar Phys. **190**, 107 (1999).
17. A. Klassen, H. Aurass, G. Mann, et al., Astron. Astrophys. **141**, 357 (2000).
18. D. A. Biesecker, D. C. Myers, B. J. Thompson, et al., Astrophys. J. **569**, 1009 (2002).
19. J. I. Khan and H. Aurass, Astron. Astrophys. **383**, 1018 (2002).
20. I. M. Chertok, V. V. Grechnev, H. S. Hudson, and N. V. Nitta, J. Geophys. Res. **109**, A02 112 (2004).
21. A. Warmuth, B. Vršnak, J. Magdalenić, et al., Astron. Astrophys. **418**, 1101 (2004).
22. V. V. Grechnev, I. M. Chertok, V. A. Slemzin, et al., J. Geophys. Res. **110**, A09S07 (2005).
23. I. M. Chertok and V. V. Grechnev, Astron. Zh. **82**, 180 (2005) [Astron. Rep. **49**, 155 (2005)].
24. M. J. Wills-Davey, C. E. DeForest, and J. O. Stenflo, Astrophys. J. **664**, 556 (2007).
25. C. Delannée, J.-F. Hochedez, and G. Aulanier, Astron. Astrophys. **465**, 603 (2007).
26. C. Delannée, T. Török, G. Aulanier, et al., Solar Phys. **247**, 123 (2008).
27. G. D. R. Attrill, L. K. Harra, L. van Driel-Gesztelyi, and P. Démoulin, Astrophys. J. Lett. **656**, L101 (2007).
28. A. Warmuth, B. Vršnak, J. Magdalenić, et al., Astron. Astrophys. **418**, 1117 (2004).
29. K. P. Dere, G. E. Brueckner, R. A. Howard, et al., Solar Phys. **175**, 601 (1997).
30. V. V. Grechnev, A. M. Uralov, V. G. Zandanov, et al., Publ. Astron. Soc. Japan **58**, 69 (2006).
31. A. N. Zhukov and F. Auchère, Astron. Astrophys. **427**, 705 (2004).
32. P. F. Chen, C. Fang, and K. Shibata, Astrophys. J. **622**, 1202 (2005)
33. Z. Švestka, Space Sci. Rev. **95**, 135 (2001).
34. A. C. Sterling and R. L. Moore, Astrophys. J. **602**, 1024 (2004).

35. A. C. Sterling and R. L. Moore, Astrophys. J. **613**, 1221 (2004).
36. D. Tripathi, H. Isobe, and H. E. Mason, Astron. Astrophys. **453**, 1111 (2006).
37. Y.-Ch. Jiang, L.-P. Li, and L.-H. Yang, Chinese J. Astron. Astrophys. **6**, 345 (2006).
38. Y. Jiang, L. Yang, K. Li, and Y. Shen, Astrophys. J. **667**, L105 (2007).
39. A. C. Sterling, L. K. Harra, and R. L. Moore, Astrophys. J. **669**, 1359 (2007).
40. J. Zhang, I. G. Richardson, D. F. Webb, et al., J. Geophys. Res. **112**, A10 102 (2007).
41. J.-P. Delaboudinière, G. E. Artzner, J. Brunaud, et al., Solar Phys. **162**, 291 (1995).
42. S. Tsuneta, L. Acton, M. Bruner, et al., Solar Phys. **136**, 37 (1991).
43. G. E. Brueckner, R. A. Howard, M. J. Koomen, et al., Solar Phys. **162**, 357 (1995).
44. D. Tripathi and N.-E. Raouafi, Astron. Astrophys. **473**, 951 (2007).
45. I. M. Chertok, Astron. Zh. **83**, 76 (2006) [Astron. Rep. **50**, 68 (2006)].
46. T. A. Howard and R. A. Harrison, Solar Phys. **219**, 315 (2004).
47. A. M. Uralov, S. V. Lesovoi, V. G. Zandanov, and V. V. Grechnev, Solar Phys. **208**, 69 (2002).
48. A. J. Hundhausen, in *The Many Faces of the Sun*, Ed. by K. Strong et al. (Springer, New York, 1999), p. 143.
49. I. M. Chertok, V. N. Obridko, E. I. Mogilevsky, et al., Astrophys. J. **567**, 1225 (2002).

Translated by D. Gabuzda